Table 1 Calculated binding potential (*BP*) values using simplified reference tissue model (SRTM), Logan graphical analysis with reference tissue (LGAR), Logan graphical analysis (LGA) and one-tissue model (1TM), compared to histamine H_1 receptor (H1R) density in autopsied human brains.[20] In the frontal, temporal, occipital, parietal, and cingulate cortices, thalamus, caudate nucleus and putamen, mean ± SD of 10 ROIs (two ROIs in right and left regions for each of 5 subjects). In the midbrain, mean ± SD of 5 ROIs (one ROI for each of 5 subjects)

Brain areas	Estimated binding potential								H1R density measured *in vitro* (fmol/mg protein/0.1 nM)
	SRTM		LGAR		LGA		1TM		
	mean	%SD	mean	%SD	mean	%SD	mean	%SD	
frontal cortex	0.53	26	0.36	18	0.38	24	0.37	25	19.1
temporal cortex	0.51	14	0.47	16	0.49	25	0.49	24	23.5
parietal cortex	0.2	29	0.36	20	0.37	26	0.37	25	16.6
occipital cortex	0.35	34	0.24	21	0.25	19	0.25	16	13.2
cingulate cortex	—	—	0.39	19	0.39	20	0.4	21	22.3
thalamus	0.24	19	0.31	17	0.31	16	0.34	16	4.3
caudate nucleus	0.32	16	0.23	44	0.24	48	0.28	44	5.3
putamen	0.32	14	0.34	29	0.34	29	0.36	27	4.4
midbrain	—	—	0.16	146	0.22	110	0.14	148	2.2

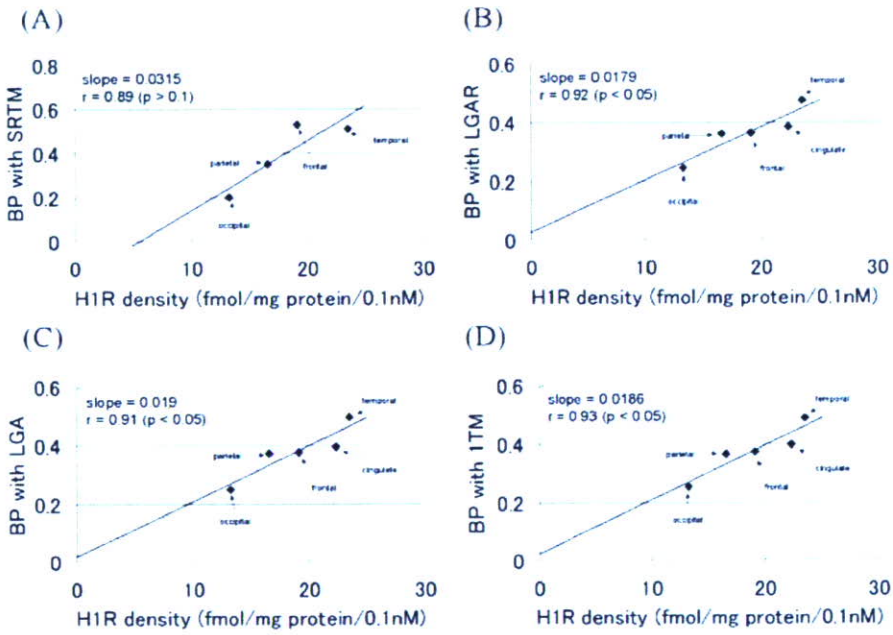

Fig. 1 Relationship between binding potential (*BP*) values and histamine H_1 receptor (H1R) densities in autopsied human brains.[20] The simplified reference tissue model (SRTM) (A), Logan graphical method with reference tissue (LGAR) (B), Logan graphical method with arterial sampling (LGA) (C), and one tissue model (1TM) (D).

sum of distribution volumes containing both nonspecific and specific bindings. The true *BP* values were calculated as $BP = DV^{ROI}/DV^{REF} - 1$. Since the DV^{ROI} value was fixed at 36.5 and DV^{REF} values were set to be changeable, high DV^{REF} values would result in low *BP* values. The parameter K_1 in the reference tissue was fixed at 0.529 [ml/g/min]. Random noise was introduced (noise level: $c = 15$) to the dynamic image data, and the noisy tTACs were analyzed with SRTM, LGAR, LGA and 1TM modeling methods at different DV^{REF} values, for which 1000 realizations of noisy tTACs were generated. Finally, the effect of nonspecific binding in the target and reference regions was evaluated by comparing *BP* estimates with the truth.

RESULTS

In the present study, *BP* values were calculated from *DV* or *DVR* values determined by each model using ROI-derived tTACs, and these *BP* values were then compared.

The mean cerebellar k_2 (0.022 [/min]) obtained by 1TM was used in LGAR. The averaged starting times t_0 for linear regression were 4.7 ± 1.7 [min] and 4.6 ± 1.8 [min] for LGA and LGAR, respectively.

Failure rate

Mean *BP* values estimated by SRTM, LGAR, LGA, and 1TM across the 5 subjects are presented in Table 1. In parameter estimation, 1TM produced reasonable *BP* values in all of 85 ROIs studied (failure rate = 0%), and LGA failed in 2 out of 85 ROIs (failure rate = 2.4%), respectively. SRTM, however, failed in 58 out of 85 ROIs (failure rate = 68.2%), while LGAR failed in only 1 out of 85 ROIs (failure rate = 1.2%).

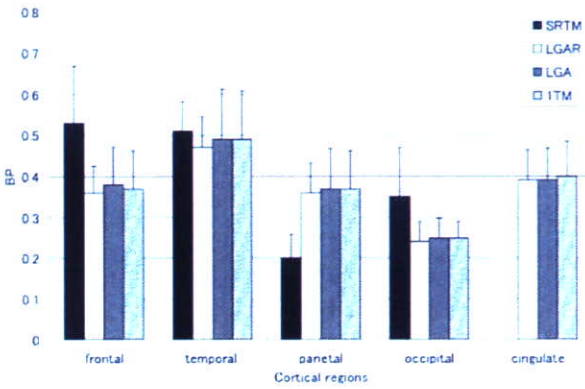

Fig. 2 Calculated binding potential (*BP*) values using simplified reference tissue model (SRTM), Logan graphical analysis with reference tissue (LGAR), Logan graphical analysis (LGA) and one-tissue model (1TM) in the five cortical regions (frontal, temporal, occipital, parietal and cingulate cortices). The *BP* value in the cingulate cortex was not available with SRTM.

Physiological rationality and correlation to results of 1TM

H1R densities in the human brain measured *in vitro* using [^{3}H]doxepin as a radioligand are given in Table 1.[20] H1R densities in the subcortical regions were lower than a quarter of the highest density in the cortex. However, a marked discrepancy in cortical/subcortical ratios was seen between the *BP* values measured *in vivo* and H1R densities measured *in vitro*. And the correlation between H1R densities and *BP* values was not statistically significant ($p > 0.05$) in the subcortical regions or in the midbrain for all of the 4 methods such as SRTM, LGAR, LGA and 1TM. Correlation of H1R densities to the *BP* values was statistically significant in the cortical regions such as the frontal, temporal, occipital, parietal and cingulate cortices, and the correlation coefficients were $r = 0.89$ ($p > 0.1$), $r = 0.92$ ($p < 0.05$), $r = 0.91$ ($p < 0.05$) and $r = 0.93$ ($p < 0.05$), respectively (Fig. 1).

In Figure 2, *BP* values in the 5 cortical regions are shown. Further correlation analysis demonstrated significant correlations of the BP values based on 1TM to those estimated by SRTM ($r = 0.73$: $p < 0.001$), LGAR ($r = 0.94$: $p < 0.001$) and by LGA ($r = 0.99$: $p < 0.001$), respectively

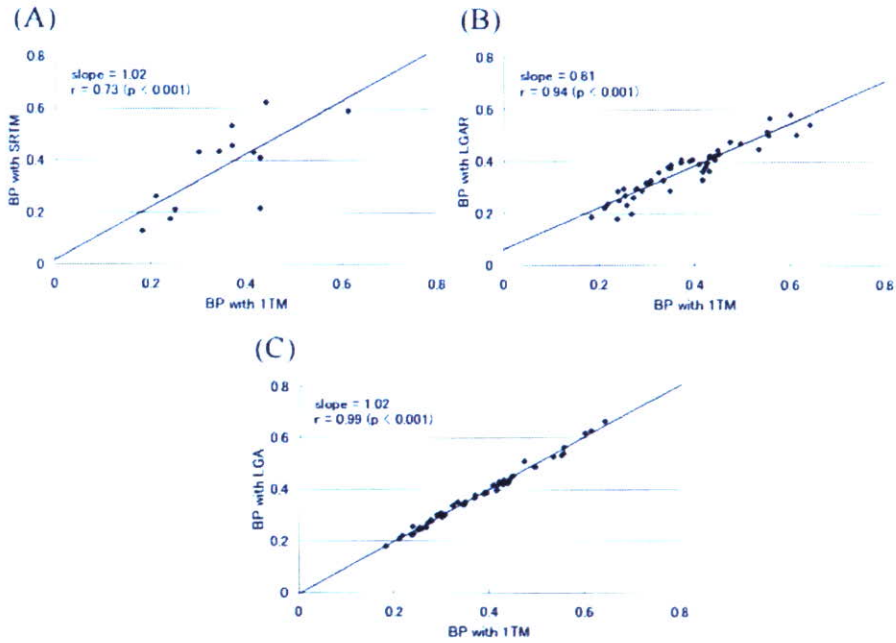

Fig. 3 Correlations between binding potential (*BP*) values calculated by 1TM and other three methods: the simplified reference tissue model (SRTM) (A), Logan graphical method with reference tissue (LGAR) (B), and Logan graphical method with arterial sampling (LGA) (C).

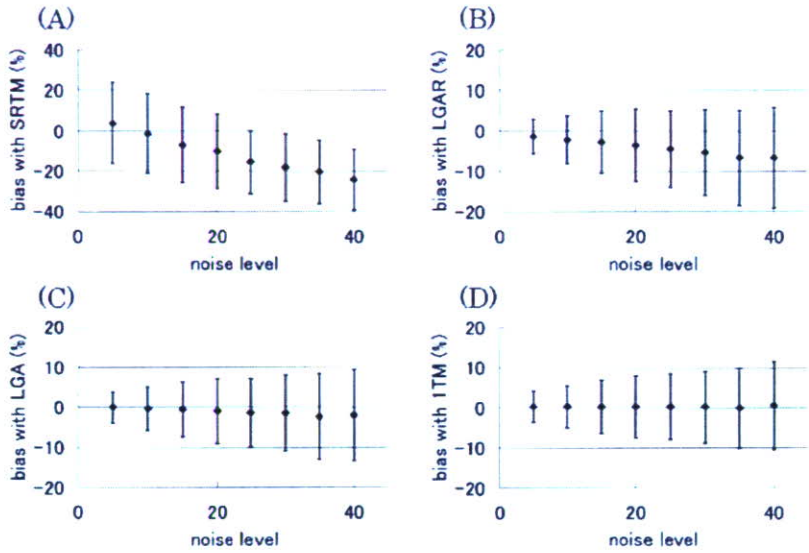

Fig. 4 Results of noise analysis in *BP* estimation in the temporal cortex with the simplified reference tissue model (SRTM) (A), Logan graphical method with reference tissue (LGAR) (B), Logan graphical method with arterial sampling (LGA) (C), and one tissue model (1TM) (D). The bias is between binding potential (*BP*) values averaged over 1000 simulations and the true *BP*. Noise level is described in MATERIALS AND METHODS section.

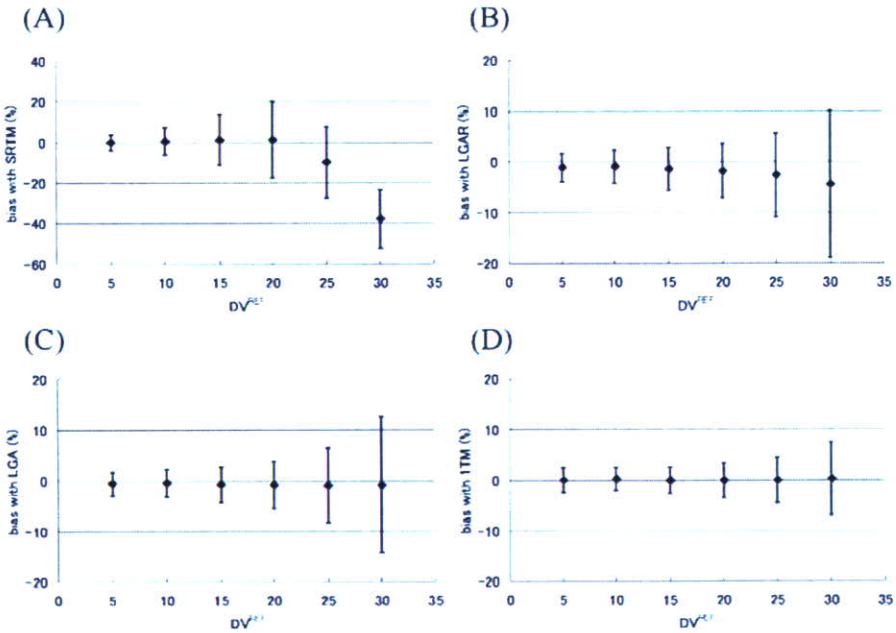

Fig. 5 Results of simulation in *BP* estimation at different DV^{REF}. The simplified reference tissue model (SRTM) (A), Logan graphical method with reference tissue (LGAR) (B), Logan graphical method with arterial sampling (LGA) (C), and one tissue model (1TM) (D). The bias is between binding potential (*BP*) values averaged over 1000 simulations and the true *BP*. Noise level *c* was fixed at 15.

(Fig. 3). The mean biases from the *BP* value based on 1TM (standard) in the cortical regions (50 ROIs: 10 ROIs for each of 5 subjects) were 6.5% with SRTM, 1.3% with LGAR and 0.3% with LGA, respectively.

Sensitivity to noise

The effect of noise in dynamic images on resultant *BP* values was examined for SRTM, LGAR, LGA and 1TM using simulation analysis. Simulated datasets were gener-

ated using TACs in the cerebellum (1TM, $K_1 = 0.529$ [ml/g/min], $k_2 = 0.0220$ [/min]), in the temporal cortex (1TM, $K_1 = 0.495$ [ml/g/min], $k_2 = 0.0140$ [/min]) and in the occipital cortex (1TM, $K_1 = 0.461$ [ml/g/min], $k_2 = 0.0153$ [/min]). Figure 4 shows results of the simulation for *BP* estimation in the temporal cortex. At all the noise levels studied here, the mean bias of *BP* values in 1TM was demonstrated to be smaller than in those of SRTM, LGAR and in LGA for both the temporal and the occipital cortices.

Simulation study on nonspecific binding

Figure 5 shows the results of simulation concerning *BP* estimation at different DV^{REF} values. As to the parameter estimation based on 1TM, biases were very small at all DV^{REF} values. In contrast, a trend toward an increased bias was observed with higher DV^{REF} values for LGA, LGAR and SRTM. Particularly, biases of SRTM at high DV^{REF} values were the largest among the all the methods examined. The results indicated that the failure rate of SRTM clearly increased with increased DV^{REF} values (for instance, 20, 25 and 30) ranging from 1.9, 28.0 to 66.5%, respectively, though the failure rate remained 0% when the DV^{REF} was smaller than 15. On the other hand, failure rates of 1TM, LGA and LGAR were always 0% at all given DV^{REF} values.

DISCUSSION

In the present study, the authors examined *BP* values estimated by SRTM and LGAR in terms of parameter stability and of correlation between autopsy data and *BP* values estimated by 1TM. An analytical method requiring arterial blood sampling is most accurate as the minimum bias and the highest correlation coefficients appear in the comparison of 1TM and LGA. However, it is difficult to apply this method to subjects in some situations such as in the presence of blood-borne infections.[15] Using reference tissue models, blood sampling and time-consuming metabolite measurements can be avoided and scanning protocol and data analysis can be simplified.[14]

Simplified reference tissue model (SRTM)

This method has been widely accepted and used for various tracers; however, this method was demonstrated to be unstable in parameter estimation of [^{11}C]doxepin binding. The failure rate of SRTM was so high (68.2%) that parameters were not available in many brain regions. The parameter correlation to 1TM was fairly low ($r = 0.71$: $p < 0.001$) and its correlation to autopsy data was not significant ($r = 0.89$: $p > 0.1$). The authors additionally tested the linear estimation method employed in Gunn's implementation of SRTM.[22] This method also failed to obtain *BP* values in 16 out of 85 ROIs (failure rate = 18.8%) even when the criterion 4 (standard error of the estimated parameter larger than 30%) was not applied. A possible reason for the high failure rate in parameter estimation with SRTM might be due to the relatively high nonspecific binding that resulted in a relatively large *DV* value in the cerebellum, which exceeded a half of the cortical *DV* values[5,12] (Table 2). Since *DV* values represent total binding, the cerebellar *DV* includes nonspecific binding while the cortical *DV* includes both specific and nonspecific bindings. Even if the amount of nonspecific binding is equal in the cortex and the cerebellum as described previously,[12] relatively high nonspecific binding might obscure the signals of specific binding in the cortex. According to Jensen and colleagues, SRTM seemed to be unsuitable for kinetic analysis for the binding of a serotonin transporter antagonist, [^{11}C]-NS 4194, because of its high nonspecific binding throughout the brain.[23]

Table 2 Calculated distribution volume (*DV*) values using Logan graphical analysis (LGA) and one-tissue model (1TM)

Brain areas	Present study *DV*			
	LGA		1TM	
	mean	%SD	mean	%SD
frontal cortex	33.6	19.4	33.6	19.7
temporal cortex	36.5	20.5	36.4	20.0
parietal cortex	33.5	18.9	33.4	19.2
occipital cortex	30.4	15.9	30.5	15.9
cingulate cortex	33.9	16.7	34.1	17.1
thalamus	32.0	16.1	32.5	15.3
caudate nucleus	30.3	20.6	31.4	21.3
putamen	32.7	19.4	33.2	19.3
midbrain	27.1	15.2	27.4	15.3
cerebellum	24.3	15.6	24.3	15.6

Thus, an additional simulation analysis was conducted in the present study in order to investigate the effect of nonspecific binding on the results of parameter estimation. The simulation analysis demonstrated that high nonspecific binding was associated with a high failure rate due to a large error in parameter estimation with SRTM, even when all required assumptions were fulfilled for the use of this model. The high failure rate due to high nonspecific binding can be predicted by the equation (2), where the high nonspecific binding reflects low k_2 values. Suppose the k_2 value is extremely low, the first term in the right-hand side is dominant and the right-hand side is almost independent of the second term which contains *BP*, k_2 and R_1. This would be one of the reasons parameters cannot be estimated uniquely. The mean k_2 value measured for [^{11}C]doxepin in the cerebellum was low ($k_2 = 0.022$ [/min]) as compared with that of other neuroreceptor radioligands such as the D_2-receptor antagonist [^{11}C]raclopride (0.163 [/min]) and the D_1-receptor antagonist [^{11}C]SCH23390 (0.101 [/min]).[24] Generally, SRTM appears to be suitable for tracers with negligibly low nonspecific binding in the reference tissues such as [^{11}C]raclopride and [^{11}C]SCH23390, but is not suitable for tracers with relatively high nonspecific binding

throughout the brain such as [^{11}C]doxepin.[14]

Logan graphical analysis with reference tissue (LGAR)
This method[15] was introduced as an extended version of LGA[11] where tracer binding was evaluated as *DVR*. However, in order to calculate *BP* values expressed by *DVR* − 1, the two following assumptions are required.

The first assumption is that the region used as the reference is devoid of specific binding. Blocking studies showed that there is no appreciable difference in [^{11}C]doxepin binding in the cerebellum with or without administration of *d*-chlorpheniramine, a highly potent H1R antagonist[4,5] demonstrating that specific binding of [^{11}C]doxepin in the cerebellum is negligibly small. In addition, postmortem human studies revealed that the H1R density in the cerebellum was less than a tenth of that in the frontal cortex.[20,25] Thus, it appears that the first assumption is justified in the present case.

The second assumption states that K_1/k_2 should be equal in the target and reference tissues. It is impossible to directly prove that K_1/k_2 is equal in all the brain regions in the case of [^{11}C]doxepin since K_1, k_2, k_3 and k_4 were not available with 2TM.[12] However, a previous study demonstrated a similar amount of nonspecific binding in the cerebellum and cerebral cortices.[25] Thus the second assumption holds for the cortical tissues, and it appears to justify calculation of *BP* values with LGAR.

Furthermore, the excellent correlation between *BP* values estimated by LGAR and 1TM ($r = 0.96$: $p < 0.001$) justifies the use of the cerebellar ROI value as a reference input. The failure rates, one of the criteria for validation of these modeling methods, were 1.2%, 2.4% and 0% for LGAR, LGA and 1TM, respectively. Because the graphical analysis requires no apriori choice of compartment configuration, the correlation to *DV* values calculated by LGA is a possible criterion for choosing a compartment configuration.

The noise simulation demonstrated that 1TM provided better parameter estimation than LGA in the presence of noise (Fig. 4). In addition, the failure rate of 1TM was 0% and the correlation between *BP* with 1TM and biopsy data in the cortical regions was strong ($r = 0.93$). As described previously, 1TM described [^{11}C]doxepin kinetics better than 2TM.[12] Therefore, we chose 1TM as the reference in the present study. Comparison between H1R densities and *BP* values from LGAR, LGA and 1TM showed much better correlations in the cortical regions than in other brain regions. One of the reasons to explain this might be relatively high nonspecific binding in these regions.[25] Therefore, the parameters in the regions with high nonspecific binding should be evaluated with caution. On the other hand, since specific binding in the cortex is relatively high, *BP* estimation in the cortex is more reliable.

In the simulations to evaluate stability to noise, the bias of *BP* values from LGAR is larger than those obtained from LGA and 1TM at all noise levels. To determine the noise level corresponding to the noise level in actual brain image data, we compared the mean sum of squares of residuals in simulation data at each noise level to the ones of the actual image datasets. For *BP* estimation in the temporal cortex with LGAR, this comparison revealed that the noise level of actual brain image data corresponds to a noise level of 10 to 15 (Fig. 4) resulting in average bias of −2.2% to −2.8%. On the other hand, for *BP* estimation in the occipital cortex with LGAR, the noise level of actual brain image data corresponded to noise levels of 10 to 15 resulting here in average bias of −3.1% to −3.7%. These results suggest that reliable parameter estimation with small bias is provided by LGAR as long as the noise level of actual brain data remains around 10 to 15 in the cortex, although LGAR underestimates the true values, when the noise level of actual brain data is higher, as mentioned already.[26]

In summary, in the present study, we analyzed [^{11}C]doxepin binding with SRTM, LGAR, LGA and 1TM. Comparison of *BP* values estimated by LGAR showed an excellent correlation with 1TM. On the other hand, SRTM did not provide satisfactory parameter estimation in several brain regions. At the noise level of actual brain data, LGAR was able to provide reliable parameter estimation in the cortex with small bias. Since LGAR does not require arterial blood sampling, this method is a useful tool for clinical studies for H1R quantification with PET and [^{11}C]doxepin. This method can be applied to investigation of brain H1R densities in various physiological and pharmacological conditions in healthy and diseased subjects in the near future, although the present study used only a limited number of normal subjects ($n = 5$). We expect a growing number of nuclear medicine techniques will be applied in related fields using convenient methods as discussed in this paper.

ACKNOWLEDGMENTS

This work was partly supported by Grants-in-Aid from the Ministry of Education, Culture, Sports, Science, and Technology, and from the Ministry of Health, Labor and Welfare, Japan. The authors thank the volunteers in the PET measurement, Keiichi Oda, Ph.D. and Ms. Miyoko Ando for their help in PET measurements and Toru Sasaki, Ph.D. and Kazunori Kawamura, Ph.D. for the preparation of [^{11}C]doxepin. The authors also thank Professor Masatoshi Itoh, at Tohoku University Cyclotron and Radioisotope Center, for his valuable comments and advice.

REFERENCES

1. Haas H, Panula P. The role of histamine and the tuberomamillary nucleus in the nervous system. *Nat Rev Neurosci* 2003; 4 (2): 121–130.
2. Yanai K, Okamura N, Tagawa M, Itoh M, Watanabe T. New findings in pharmacological effects induced by antihista-

mines: from PET studies to knock-out mice. *Clin Exp Allergy* 1999; 29 Suppl 3: 29–36; discussion 37–38.
3. Huang ZL, Qu WM, Li WD, Mochizuki T, Eguchi N, Watanabe T, et al. Arousal effect of orexin A depends on activation of the histaminergic system. *Proc Natl Acad Sci USA* 2001; 98 (17): 9965–9970.
4. Yanai K, Watanabe T, Yokoyama H, Meguro K, Hatazawa J, Itoh M, et al. Histamine H_1 receptors in human brain visualized *in vivo* by [^{11}C]doxepin and positron emission tomography. *Neurosci Lett* 1992; 137 (2): 145–148.
5. Ishiwata K, Kawamura K, Wang WF, Tsukada H, Harada N, Mochizuki H, et al. Evaluation of *in vivo* selective binding of [^{11}C]doxepin to histamine H_1 receptors in five animal species. *Nucl Med Biol* 2004; 31 (4): 493–502.
6. Higuchi M, Yanai K, Okamura N, Meguro K, Arai H, Itoh M, et al. Histamine H(1) receptors in patients with Alzheimer's disease assessed by positron emission tomography. *Neuroscience* 2000; 99 (4): 721–729.
7. Iinuma K, Yokoyama H, Otsuki T, Yanai K, Watanabe T, Ido T, et al. Histamine H_1 receptors in complex partial seizures. *Lancet* 1993; 341 (8839): 238.
8. Yanai K, Ryu JH, Watanabe T, Iwata R, Ido T, Sawai Y, et al. Histamine H_1 receptor occupancy in human brains after single oral doses of histamine H_1 antagonists measured by positron emission tomography. *Br J Pharmacol* 1995; 116 (1): 1649–1655.
9. Tagawa M, Kano M, Okamura N, Higuchi M, Matsuda M, Mizuki Y, et al. Neuroimaging of histamine H_1-receptor occupancy in human brain by positron emission tomography (PET): a comparative study of ebastine, a second-generation antihistamine, and (+)-chlorpheniramine, a classical antihistamine. *Br J Clin Pharmacol* 2001; 52 (5): 501–509.
10. Tashiro M, Sakurada Y, Iwabuchi K, Mochizuki H, Kato M, Aoki M, et al. Central Effects of Fexofenadine and Cetirizine: Measurement of Psychomotor Performance, Subjective Sleepiness, and Brain Histamine H_1-Receptor Occupancy Using ^{11}C-Doxepin Positron Emission Tomography. *J Clin Pharmacol* 2004; 44 (8): 890–900.
11. Logan J, Fowler JS, Volkow ND, Wolf AP, Dewey SL, Schlyer DJ, et al. Graphical analysis of reversible radioligand binding from time-activity measurements applied to [*N*-^{11}C-methyl]-(−)-cocaine PET studies in human subjects. *J Cereb Blood Flow Metab* 1990; 10 (5): 740–747.
12. Mochizuki H, Kimura Y, Ishii K, Oda K, Sasaki T, Tashiro M, et al. Quantitative measurement of histamine H(1) receptors in human brains by PET and [^{11}C]doxepin. *Nucl Med Biol* 2004; 31 (2): 165–171.
13. Mochizuki H, Kimura Y, Ishii K, Oda K, Sasaki T, Tashiro M, et al. Simplified PET measurement for evaluating histamine H_1 receptors in human brains using [^{11}C]doxepin. *Nucl Med Biol* (in press).
14. Lammertsma AA, Hume SP. Simplified reference tissue model for PET receptor studies. *Neuroimage* 1996; 4 (3 Pt 1): 153–158.
15. Logan J, Fowler JS, Volkow ND, Wang GJ, Ding YS, Alexoff DL. Distribution volume ratios without blood sampling from graphical analysis of PET data. *J Cereb Blood Flow Metab* 1996; 16 (5): 834–840.
16. Mintun MA, Raichle ME, Kilbourn MR, Wooten GF, Welch MJ. A quantitative model for the *in vivo* assessment of drug binding sites with positron emission tomography. *Ann Neurol* 1984; 15 (3): 217–227.
17. Koeppe RA, Holthoff VA, Frey KA, Kilbourn MR, Kuhl DE. Compartmental analysis of [^{11}C]flumazenil kinetics for the estimation of ligand transport rate and receptor distribution using positron emission tomography. *J Cereb Blood Flow Metab* 1991; 11 (5): 735–744.
18. Phelps ME, Huang SC, Hoffman EJ, Kuhl DE. Validation of tomographic measurement of cerebral blood volume with C-11-labeled carboxyhemoglobin. *J Nucl Med* 1979; 20 (4): 328–334.
19. Carson RE, Parameters estimation in positron emission tomography. In: *Positron emission tomography. Principles and applications for the brain and the heart*. Phelps ME, Mazziotta JC, Schelbert HR (eds). New York; Raven Press, 1986: 347–390.
20. Kanba S, Richelson E. Histamine H_1 receptors in human brain labelled with [^{3}H]doxepin. *Brain Res* 1984; 304 (1): 1–7.
21. Kimura Y, Senda M, Alpert NM. Fast formation of statistically reliable FDG parametric images based on clustering and principal components. *Phys Med Biol* 2002; 47 (3): 455–468.
22. Gunn RN, Lammertsma AA, Hume SP, Cunningham VJ. Parametric imaging of ligand-receptor binding in PET using a simplified reference region model. *Neuroimage* 1997; 6 (4): 279–287.
23. Jensen SB, Smith DF, Bender D, Jakobsen S, Peters D, Nielsen EO. [^{11}C]-NS 4194 versus [^{11}C]-DASB for PET imaging of serotonin transporters in living porcine brain. *Synapse* 2003; 49: 170–177.
24. Sossi V, Holden JE, Chan G, Krzywinski M, Stoessl AJ, Ruth TJ. Analysis of four dopaminergic tracers kinetics using two different tissue input function methods. *J Cereb Blood Flow Metab* 2000; 20 (4): 653–660.
25. Yanai K, Watanabe T, Meguro K, Yokoyama H, Sato I, Sasano H, et al. Age-dependent decrease in histamine H_1 receptor in human brains revealed by PET. *Neuroreport* 1992; 3 (5): 433–436.
26. Logan J, Fowler JS, Ding YS, Franceschi D, Wang GJ, Volkow ND, et al. Strategy for the formation of parametric images under conditions of low injected radioactivity applied to PET studies with the irreversible monoamine oxidase A tracers [^{11}C]clorgyline and deuterium-substituted [^{11}C]clorgyline. *J Cereb Blood Flow Metab* 2002; 22 (11): 1367–1376.

doi:10.1093/brain/awh702 *Brain* (2006), **129**, 399–410

The association between the Val158Met polymorphism of the catechol-*O*-methyl transferase gene and morphological abnormalities of the brain in chronic schizophrenia

Takashi Ohnishi,[1,2,4] Ryota Hashimoto,[2] Takeyuki Mori,[1,2] Kiyotaka Nemoto,[1] Yoshiya Moriguchi,[1] Hidehiro Iida,[4] Hiroko Noguchi,[2] Tetsuo Nakabayashi,[2,3] Hiroaki Hori,[2,3] Mayu Ohmori,[3] Ryoutaro Tsukue,[3] Kimitaka Anami,[3] Naotugu Hirabayashi,[3] Seiichi Harada,[3] Kunimasa Arima,[3] Osamu Saitoh[3] and Hiroshi Kunugi[2]

[1]Department of Radiology, National Center Hospital of Mental, Nervous and Muscular Disorders, National Center of Neurology and Psychiatry, [2]Department of Mental Disorder Research, National Institute of Neuroscience, National Center of Neurology and Psychiatry, [3]Department of Psychiatry, National Center Hospital of Mental, Nervous, and Muscular Disorders, National Center of Neurology and Psychiatry, Tokyo and [4]Department of Investigative Radiology, Research Institute, National Cardiovascular Center, Osaka, Japan

Correspondence to: Takashi Ohnishi, Department of Radiology, National Center Hospital of Mental, Nervous, and Muscular Disorders, National Center of Neurology and Psychiatry 4-1-1 Ogawa Higashi, Kodaira City, Tokyo, Japan 187-0031
E-mail: tohnishi@hotmail.com

The catechol-*O*-methyl transferase (COMT) gene is considered to be a promising schizophrenia susceptibility gene. A common functional polymorphism (Val158Met) in the COMT gene affects dopamine regulation in the prefrontal cortex (PFC). Recent studies suggest that this polymorphism contributes to poor prefrontal functions, particularly working memory, in both normal individuals and patients with schizophrenia. However, possible morphological changes underlying such functional impairments remain to be clarified. The aim of this study was to examine whether the Val158Met polymorphism of the COMT gene has an impact on brain morphology in normal individuals and patients with schizophrenia. The Val158Met COMT genotype was obtained for 76 healthy controls and 47 schizophrenics. The diagnostic effects, the effects of COMT genotype and the genotype-diagnosis interaction on brain morphology were evaluated by using a voxel-by-voxel statistical analysis for high-resolution MRI, a tensor-based morphometry. Patients with schizophrenia demonstrated a significant reduction of volumes in the limbic and paralimbic systems, neocortical areas and the subcortical regions. Individuals homozygous for the Val-COMT allele demonstrated significant reduction of volumes in the left anterior cingulate cortex (ACC) and the right middle temporal gyrus (MTG) compared to Met-COMT carriers. Significant genotype-diagnosis interaction effects on brain morphology were noted in the left ACC, the left parahippocampal gyrus and the left amygdala-uncus. No significant genotype effects or genotype-diagnosis interaction effects on morphology in the dorsolateral PFC (DLPFC) were found. In the control group, no significant genotype effects on brain morphology were found. Schizophrenics homozygous for the Val-COMT showed a significant reduction of volumes in the bilateral ACC, left amygdala-uncus, right MTG and left thalamus compared to Met-COMT schizophrenics. Our findings suggest that the Val158Met polymorphism of the COMT gene might contribute to morphological abnormalities in schizophrenia.

Keywords: schizophrenia; polymorphism; COMT; ACC; DLPFC

Abbreviations: ACC = anterior cingulate cortex; COMT = catechol-*O*-methyl transferase; DLPFC = dorsolateral prefrontal cortex; FDR = false discovery rate; IQ = intelligence quotient; JART = Japanese version of National Adult Reading Test; ROI = region of interest; SPM = statistical parametric mapping; TBM = tensor-based morphometry

Received July 15, 2005. Revised September 21, 2005. Accepted October 27, 2005. Advance Access publication December 5, 2005

Introduction

Schizophrenia is a severe neuropsychiatric disorder with deficits of multiple domains of cognitive functions, volition and emotion. Family and twin studies have provided cumulative evidence for a genetic basis of schizophrenia (Kendler, 1983; McGue *et al.*, 1983; Sullivan *et al.*, 2003); however, identification of the underlying susceptibility loci has been limited. Collective data have suggested that the aetiology of schizophrenia involves the interplay of complex polygenic influences and environmental risk factors operating on brain maturational processes (Harrison *et al.*, 2005).

In vivo neuroimaging studies have demonstrated that brain abnormalities should play an important role in the pathophysiology of schizophrenia. Structural MRI studies have demonstrated relatively consistent brain abnormalities in patients with schizophrenia, such as enlargement of the ventricular system and regional volume decrease in the temporal lobe structures (Gaser *et al.*, 2001; Okubo *et al.*, 2001; Shenton *et al.*, 2001; Davidson and Heinrichs, 2003). Studies with schizophrenics and their healthy siblings demonstrate that even healthy siblings share some of morphological abnormalities observed in schizophrenia (Steel *et al.*, 2002; Gogtay *et al.*, 2003). A recent morphological MR study revealed that a common polymorphism of the brain-derived neurotrophic factor, one of the well-known schizophrenia susceptibility genes, affected the anatomy of the hippocampus and prefrontal cortex (PFC) in healthy individuals (Pezawas *et al.*, 2004). Furthermore, some studies have suggested that environmental factors interact with genetic factors (Cannon *et al.*, 1993; Nelson *et al.*, 2004). For example, obstetric complications are well known non-genetic risk factors of schizophrenia. However, a previous study suggested that obstetric complications might induce brain morphological abnormalities in schizophrenics and their siblings, but not in comparison with subjects at low genetic risk for schizophrenia (Cannon *et al.*, 1993). These facts suggest that genetic factors should have considerable impact on brain morphology in patients with schizophrenia.

Catechol-*O*-methyl transferase (COMT) is a promising schizophrenia susceptibility gene because of its role in monoamine metabolism (Goldberg *et al.*, 2003; Stefanis *et al.*, 2004; Harrison *et al.*, 2005). A common single nucleotide polymorphism (SNP) of the COMT gene producing an amino acid substitution of methionine (met) to valine (val) at position 108/158 (Val158Met) affects dopamine regulation in the PFC (Palmatier *et al.*, 1999). This polymorphism impacts on the stability of the enzyme, such that the Val-COMT allele has significantly lower enzyme activity than the Met-COMT allele (Weinberger *et al.*, 2001; Chen *et al.*, 2004). Several studies have revealed that the Val-COMT allele is associated with poorer performances, compared to the Met-COMT allele, in cognitive tasks of frontal function such as the Wisconsin Card Sorting Test (WCST) and N-back task (Egan *et al.*, 2001; Weinberger *et al.*, 2001; Goldberg *et al.*, 2003). The underlying mechanism of such behavioural differences may be related to lower prefrontal dopamine levels arising from higher dopamine catabolism mediated by the Val-COMT allele (Chen *et al.*, 2004; Tunbridge *et al.*, 2004).

The results of studies on the association between the Val158Met polymorphism and schizophrenia have, however, been controversial (Daniels *et al.*, 1996; Kunugi *et al.*, 1997; Ohmori *et al.*, 1998; Norton *et al.*, 2002; Galderisi *et al.*, 2005; Ho *et al.*, 2005). The result of a meta-analysis was even more inconclusive (Fan *et al.*, 2005). Such inconsistency was also found in associations between frontal functions and the Val158Met polymorphism (Egan *et al.*, 2001; Weinberger *et al.*, 2001; Goldberg *et al.*, 2003; Ho *et al.*, 2005). The possible morphological changes due to the COMT gene might be present and play a role in susceptibility to schizophrenia and in giving rise to impaired frontal functions. However, morphological changes underlying functional impairments remain to be clarified.

A recent advancement of methods for MR volumetry, such as voxel-based morphometry and deformation-based morphometry [or tensor-based morphometry (TBM)], allows us to explore and analyse brain structures of schizophrenics (Wright *et al.*, 1995; Gaser *et al.*, 2001). Using TBM techniques, we investigated the association between the Val158-Met polymorphism of the COMT gene and brain morphology in normal individuals and patients with schizophrenia. The aim of this study was to clarify whether there are significant genotype and/or genotype-disease interaction effects on brain morphology.

Methods

Subjects

Seventy-six healthy subjects and forty-seven patients with schizophrenia participated in the study. All the subjects were biologically unrelated Japanese. Written informed consent was obtained from all the subjects in accordance with ethical guidelines set by a local ethical committee. All normal subjects were screened using a questionnaire on medical history and excluded if they had neurological, psychiatric or medical conditions that could potentially affect the CNS, such as substance abuse or dependence, atypical headache, head trauma with loss of consciousness, asymptomatic or symptomatic cerebral infarctions detected by T_2-weighted MRI, hypertension, chronic lung

disease, kidney disease, chronic hepatic disease, cancer, or diabetes mellitus. The patients were diagnosed on the basis of DSM-IV criteria, information from medical records and a clinical interview. All patients were stable and/or partially remitted at the time of MR measurement and neuropsychological tests.

According to genotypes, each group (control and schizophrenia) was categorized into three groups; the homozygous Val-COMT group (control: n = 38, two were left-handed, schizophrenia: n = 19, one was left-handed), the Val/Met-COMT group (control: n = 25, three were left-handed, schizophrenia: n = 22, all were right-handed) and the remaining homozygous Met-COMT group (control: n = 13, all were right-handed, schizophrenia: n = 6, all were right-handed). Because of the small number of subjects with homozygous Met-COMT, the Val/Met-COMT and homozygous Met-COMT groups were combined and treated as one group, the Met-COMT carriers. Table 1 shows the characteristics of each group. All groups were of comparable age, gender (χ^2 test, df = 3, P = 0.38) and handedness (χ^2-test, df = 3, P = 0.53). No genotype effects and genotype-diagnosis interaction effects were found in years of education, scores of full scale Intelligence Quotient (IQ) and scores of premorbid IQ [Japanese version of National Adult Reading Test (JART) score], however, patients who had fewer years of education ($P < 0.0001$), had lower scores of both full scale IQ and JART ($P < 0.001$). The duration of illness, medication and hospitalization, the age at disease onset and drug dose (chlorpromazine equivalent) of those homozygous for the Val-COMT did not differ from the Met-COMT carriers.

SNP genotyping

Venous blood was drawn from subjects and genomic DNA was extracted from whole blood according to the standard procedures. The Val158Met polymorphism of the COMT gene (dbSNP accession: rs4680) was genotyped using the TaqMan 5′-exonuclease allelic discrimination assay, described previously (Hashimoto *et al.*, 2004, 2005). Briefly, primers and probes for detection of the SNP are: forward primer 5′-GACTGTGCCGCCATCAC-3′, reverse primer 5′-CAGGCATGCACACCTTGTC-3′, probe 1 5′-VIC-TTTCGCTG-GCGTGAAG-MGB-3′ and probe 2 5′-FAM-CGCTGGCATGAAG-MGB-3′. PCR cycling conditions were: at 95°C for 10 min, 50 cycles of 92°C for 15 s and 60°C for 1 min.

MRI procedures

All MR studies were performed on a 1.5 tesla Siemens Magnetom Vision plus system. A three dimensional (3D) volumetric acquisition of a T_1-weighted gradient echo sequence produced a gapless series of thin sagittal sections using an MPRage sequence (TE/TR, 4.4/11.4 ms; flip angle, 15°; acquisition matrix, 256 × 256; 1 NEX, field of view, 31.5 cm; slice thickness, 1.23 mm).

Image analysis (TBM)

The basic principle of TBM is to analyse the local deformations of an image and to infer local differences in brain structure. In TBM, MRI scans of individual subjects are mapped to a template image with three-dimensional (3D) non-linear normalization routines. Local deformations were estimated by a univariate Jacobian approach. The basic principle of TBM is the same as a method used in a previous report described as deformation-based morphometry (Gaser *et al.*, 2001). Firstly, inhomogeneities in MR images were corrected using a bias correction function in statistical parametric mapping (SPM2), then the corrected image was scalp-edited by masking with a probability image of brain tissue obtained from each image using a segmentation function in SPM2. Using a linear normalization algorithm in SPM2, all brains were resized to a voxel size of 1.5 mm and adjusted for orientation and overall width, length and height (Fig. 1A). Therefore, brains were transformed to the anatomical space of a template brain whose space is based on Talairach space (Talairach and Tournoux, 1988). Subsequent non-linear normalization introduced local deformations to each brain to match it to the same scalp-edited template brain (Fig. 1C). The non-linear transformation was done using the high-dimension-warping algorithm (Ashburner and Friston, 2004). After the high dimensional warping, each image (Fig. 1B) looks similar to the template (Fig. 1C). Figure 2 demonstrated a mean MR image of 76 controls (left) and a mean MR image of 47 schizophrenics after high dimensional warping (Fig. 2). We obtained 3D deformation fields for every brain (Fig. 1D). Each of these 3D deformation fields consists of displacement vectors for every voxel, which describe the 3D displacement needed to locally deform the brain to match it to the template. We calculated the Jacobian determinants to obtain voxel by voxel parametric maps of local volume change relative to the template brain (Fig. 1E). The local Jacobian determinant is a parameter commonly used in continuum mechanics (Gurtin, 1987), which characterizes volume changes, such as local shrinkage or enlargement caused by warping. The parametric maps of Jacobian determinants were analysed using SPM2, which implements a 'general linear model'. To test hypotheses about regional population effects and interaction, data were analysed by an analysis of covariance (ANCOVA) without global normalization. There was no significant difference in age among the four groups, however, patients with schizophrenia, particularly those homozygous for the Val-COMT allele, were older than controls. Therefore, we treated age and years of education and scores of JART as nuisance variables. Since TBM explores the entire brain (grey matter, CSF space and white matter) at once, the search volume of TBM has a large number of voxels and since our interest was in morphological changes in the grey matter and CSF space, we excluded white matter tissue from analyses by using an explicit mask (Fig. 1F). We used $P < 0.001$, corrected for multiple comparisons with false discovery rate (FDR) <0.05 as a statistical threshold. The resulting sets of t values constituted the statistical parametric maps {SPM (t)}. Firstly, we estimated the main effects, the genotype effect in total subjects (the Val/Val-COMT versus the Met-COMT carriers) and the diagnostic effect (schizophrenia versus controls) and then the genotype-diagnosis interaction effect was estimated. Furthermore, the effects of genotypes in each group (controls carrying the Val/Val-COMT gene versus controls carrying the Met-COMT gene and schizophrenics carrying the Val/Val-COMT gene versus schizophrenics carrying the Met-COMT gene) were estimated within the ANCOVA design matrix. Anatomical localization accorded both to MNI coordinates and Talairach coordinates obtained from M. Brett's transformations (www.mrc-cbu.cam.ac.uk/Imaging/mnispace.html) and are presented as Talairach coordinates (Talairach and Tournoux, 1988). Since previous studies have demonstrated the association between the Val158Met polymorphism and the dorsolateral PFC (DLPFC), we applied an additional hypothesis-driven region of interest (ROI) method to test regional population effects in the DLPFC. For this ROI analysis, we used the Wake Forest University PickAtlas (Maldjian *et al.*, 2003) within the ANCOVA design matrix for SPM analysis. We set $P < 0.05$ (uncorrected) with a small volume correction ($P < 0.05$ within the ROI) to assess grey matter volume changes in the DLPFC (Brodmann area 46, 9 and 8).

Table 1 Subject characteristics

	Control Val/Val	Met carriers	Schizophrenia Val/Val	Met carriers	Diagnosis F (P)	Genotype F (P)*	Genotype by diagnosis F (P)
Number of subjects	38	38	19	28			
Gender (M/F)	16 out of 22	14 out of 24	11 out of 8	13 out of 15			
Handedness (R/L)	36 out of 2	35 out of 3	18 out of 1	28 out of 0			
Age (years)	41.47 (13.42)	39.26 (10.6)	45.98 (15.29)	43.05 (10.57)	3.633 (0.059)	1.7 (0.195)	0.21 (0.647)
Education (years)	17 (3.16)	16.06 (2.57)	12.67 (2.43)	13.33 (3.31)	30.855 (<0.0001)	0.047 (0.828)	1.61 (0.208)
Full scale IQ (WAIS-R)	113.42 (12.05)	108.93 (13.58)	80.69 (17.68)	88.958 (22.08)	57.9 (<0.001)	0.29 (0.59)	3.41 (0.068)
JART	78.8 (10.45)	75.42 (13.65)	54.69 (20.74)	62.25 (27.06)	23.366 (<0.001)	0.292 (0.59)	2.014 (0.159)
Wechsler Memory Scale—Revised							
Verbal memory	111.78 (15.001)	111.061 (12.89)	78.0 (21.623)	81.33 (18.57)	86.93 (<0.001)	0.147 (0.702)	0.354 (0.553)
Visual memory	112.1 (8.51)	106.55 (11.99)	74.78 (24.32)	83.29 (20.613)	85.51 (<0.001)	0.204 (0.65)	4.605 (0.03)
General memory	113.31 (13.92)	110.85 (12.22)	74.43 (21.3)	79.33 (19.14)	111.93 (<0.001)	0.135 (0.715)	1.226 (0.27)
Attention/concentration	104.47 (13.25)	102.94 (16.51)	87.79 (19.09)	92.54 (17.38)	16.08 (0.001)	0.228 (0.634)	0.866 (0.14)
Delayed recall	111.88 (15.46)	112.48 (10.08)	77.07 (20.92)	81.21 (19.19)	99.74 (<0.001)	0.52 (0.475)	0.284 (0.59)
WCST (preservative error)	2.5 (3.89)	3.14 (3.90)	12.08 (11.54)	8.52 (10.63)	24.5 (<0.0001)	0.93 (0.34)	1.93 (0.17)
Digit span	11.12 (3.25)	10.77 (3.34)	7.83 (3.93)	9.09 (2.74)	12.165 (0.0007)	0.415 (0.52)	1.28 (0.261)
Onset age			25.38 (10.34)	23.74 (7.992)		0.52	
Duration of illness (years)			19.86 (14.93)	18.84 (9.8)		0.77	
Duration of hospitalization (months)			66 (153.41)	59.59 (91.18)		0.86	
Duration of medication (years)			12.86 (14.21)	16.4 (9.89)		0.29	
Drug dose of typical antipyschotic drugs (mg/day, chlorpromazine equivalent)			617.9 (720.18)	700.38 (752.67)		0.69	
Drug dose of atypical antipyschotic drugs (mg/day, chlorpromazine equivalent)			282.3 (428.29)	340.23 (482.19)		0.66	

Mean (standard deviation); WAIS-R = Wechsler Adult Intelligence Scale—Revised; JART = Japanese version of National Adult Reading Test; WCST = Wisconsin Card Sorting Test.

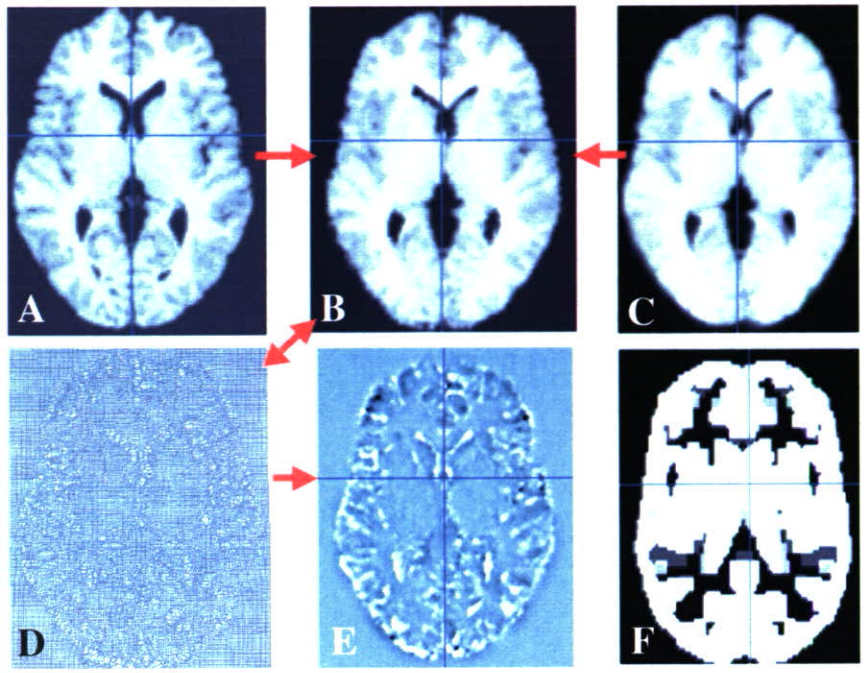

Fig. 1 Steps of analysis for tensor-based morphometry. An example is shown for a single subject in one axial slice. The single object brain (**A**) has been corrected for orientation and overall size to the template brain (**C**). Non-linear spatial normalization removes most of the anatomical differences between the two brains by introducing local deformations to the object brain, which then (**B**) looks as similar as possible to the template. Image (**D**) shows the deformations applied to the object brain by a deformed grid. Statistical analysis can be done univariate using the local Jacobian determinant as a derivative of the field (**E**). An explicit mask image (**F**) was used to explore morphology in the grey matter and CSF space.

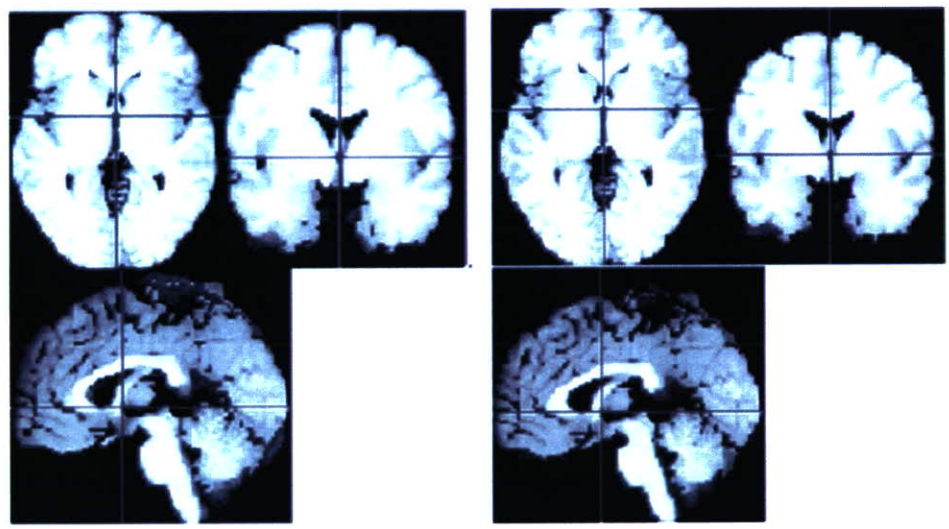

Fig. 2 Mean images after high dimensional warping control subjects and schizophrenics. *Left*: The mean image of warped MR images obtained from 76 controls. Even after averaging, the mean image is not blurred. *Right*: The mean image of warped MR images obtained from 47 schizophrenics. The mean image of schizophrenic looks similar to that of controls.

Results

Behavioural data

Patients had a lower full scale IQ, measured by the Wechsler Adult Intelligence Scale—Revised, than controls. They also had a lower expected premorbid IQ measured by a JART, lower scores of Wechsler Memory Scale—Revised and demonstrated poorer performance of working memory measures such as the number of preservative errors in the WCST and digit span (Table 1). No genotype or genotype-diagnosis interaction effects were found in working memory measures

Table 2 Results of image analyses

Anatomical regions	Brodmann area	Cluster size	Corrected P FDR	*T*-value (voxel level)	Talairach coordinates		
					x	*y*	*z*
Main effects							
Diagnosis effects (control > schizophrenia) (Fig. 3)							
Limbic system							
R insula	BA13	4682	0.000	6.41	33	11	−2
L insula	BA13	4017	0.000	8.81	−33	11	4
R parahippocampal gyrus, amygdala-uncus	BA36	4682	0.000	7.32	30	1	−17
R parahippocampal gyrus	BA36	186	0.000	5.04	30	−41	−8
L parahippocampal gyrus, hippocampus-amygdala	BA34/36	637	0.000	5.46	−20	−41	−8
R anterior cingulate cortex	BA32	147	0.000	4.9	9	33	20
L anterior cingulate cortex	BA32	200	0.000	4.63	−11	32	20
L cingulate gyrus	BA32	275	0.001	4.2	−12	−16	39
Prefrontal cortex							
R inferior frontal gyrus	BA47,11	145	0.000	4.99	27	28	−11
R superior frontal gyrus	BA8/9	1889	0.000	6.08	12	43	39
L medial frontal gyrus	BA9	1333	0.000	5.13	−8	47	19
L inferior frontal gyrus	BA45	141	0.000	4.55	−44	23	15
L middle frontal gyrus	BA8	482	0.000	4.44	−30	24	43
L superior frontal gyrus	BA8	482	0.000	4.39	−35	17	51
Premotor area							
R dorsal premotor area	BA6	429	0.000	4.37	41	13	45
Temporal cortex							
R superior temporal gyrus	BA22	806	0.000	5.04	47	−23	−1
R middle temporal gyrus	BA21	806	0.000	4.87	56	−15	−3
L superior temporal gyrus	BA38	4017	0.000	7	−36	1	−17
Central grey matter							
L thalamus		4017	0.000	7.26	−15	−17	2
Diagnosis effects (control < schizophrenia) (Fig. 4)							
L sylvian fissure		621	0.000	6.7	−45	17	−3
R sylvian fissure		774	0.000	6.59	44	17	−8
Lateral ventricle (anterior horn)		279	0.000	5.27	−5	21	4
Lateral ventricle (L inferior horn)		248	0.000	6.18	−41	−30	−10
Lateral ventricle (R inferior horn)		137	0.000	5.02	36	−40	−1
Interhemisphrenic fissure		154	0.000	5.28	3	55	−12
Genotype effects (Val/Val-COMT < Met-COMT carriers) (Fig. 5)							
Limbic system							
L anterior cingulate cortex	BA24/25	334	0.033	4.29	−8	17	−13
Temporal cortex							
R middle temporal gyrus	BA21	285	0.016	5.10	59	−3	−14
Genotype-diagnosis interaction effects (Fig. 6)							
Limbic system							
L anterior cingulate gyrus	BA24/25/32	264	0.044	3.77	−6	25	−6
L parahippocampal gyrus, amygdala-uncus	BA34	219	0.048	3.74	−24	−6	−14
The effects of polymorphism in control group (no significant difference)							
The effects of polymorphism in schizophrenia							
Val/Val-COMT < Val/Met, Met/Met-COMT (Fig. 7)							
Limbic system							
L parahippocampal gyrus, amygdala-uncus	BA28	81	0.010	4.17	−26	2	−22
L anterior cingulate cortex	BA24/25/32	263	0.007	4.38	−7	20	−8
Central grey matter							
L thalamus		91	0.014	3.94	−21	−28	6

and IQ, however, a significant genotype-by-diagnosis interaction effect was found in a visual memory measure (F = 4.605, df = 1, P = 0.03) (Table 1). However, a *post hoc t*-test (Bonferroni test) demonstrated no genotype effect in each diagnostic category (control: P = 0.15, schizophrenia: P = 0.11).

Morphological changes in schizophrenia (diagnosis effects)

In comparison with controls, patients with schizophrenia demonstrated a significant reduction of volumes in multiple brain areas, such as the limbic and paralimbic systems, neocortical areas and the subcortical regions (Table 2 and Fig. 3).

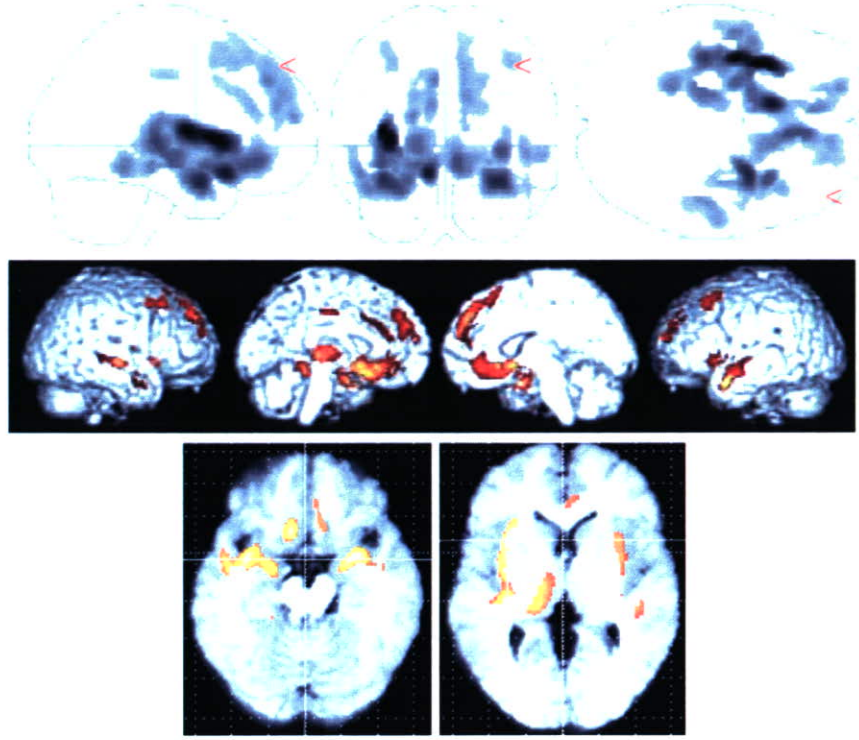

Fig. 3 Decreased volumes in schizophrenics ($n = 47$) as compared to controls ($n = 76$). *Top*: The SPM {*t*} is displayed in a standard format as a maximum-intensity projection (MIP) viewed from the right, the back and the top of the brain. The anatomical space corresponds to the atlas of Talairach and Tournoux. Representation in stereotaxic space of regions with significant reduction of volume in schizophrenia was demonstrated. Schizophrenics demonstrated a significant reduction of volumes in the multiple brain areas, such as the limbic and paralimbic systems, neocortical areas and the subcortical regions. *Middle*: The SPM {*t*} is rendered onto T_1-weighted MR images. *Bottom*: The SPM {*t*} is displayed onto axial T_1-weighted MR images. A significantly decreased volume of the amygdala-uncus, bilateral insular cortices, ACC, temporal cortex and the left thalamus in schizophrenics was noted.

In the limbic and paralimbic systems, patients with schizophrenia showed reduction of volumes in the parahippocampal gyri, amygdala-uncus, insular cortices and the anterior cingulate cortices (ACC). They also demonstrated reduced volumes in the frontal and temporal association areas, dorsal premotor areas and the left thalamus. In comparison with controls, patients with schizophrenia showed significantly increased volume in the CSF space such as lateral ventricle, sylvian and the interhemispheric fissures but not in the grey matter (Table 2 and Fig. 4).

Morphological changes associated with the Val158Met polymorphism (genotype effects)

In comparison with Met-COMT carriers, individuals homozygous for the Val-COMT allele demonstrated a significant reduction of volumes in the left ACC and the right middle temporal gyrus (MTG) (Table 2 and Fig. 5). The hypothesis-driven analysis demonstrated a genotype effect on volumes in the bilateral DLPFC (right BA9, left BA8) at a lenient threshold (uncorrected $P = 0.05$) (data are not shown), however, no voxels could survive after the correction for multiple comparisons (FDR < 0.05) within the ROI. There were no areas that individuals homozygous for the Val-COMT allele demonstrated a significant increment of volume compared to Met-COMT carriers.

Genotype—diagnosis interaction effects

We found significant genotype-diagnosis interaction effects on brain morphology. The stronger effects of Val158Met polymorphism on brain morphology in schizophrenia than those in controls were noted in the left ACC and the left amygdala-uncus (Table 2 and Fig. 6). The hypothesis-driven analysis demonstrated a genotype-diagnosis interaction effect on the volume of the right DLPFC (BA9/46) at a lenient threshold (uncorrected $P = 0.05$) (data not shown), however, no voxels could survive after the correction of multiple comparisons (FDR < 0.05) within the ROI.

Effects of the Val58Met polymorphism on brain morphology

Since genotype–disease interaction effects were found, we estimated the effects of genotypes on brain morphology in the control groups and the schizophrenic groups separately.

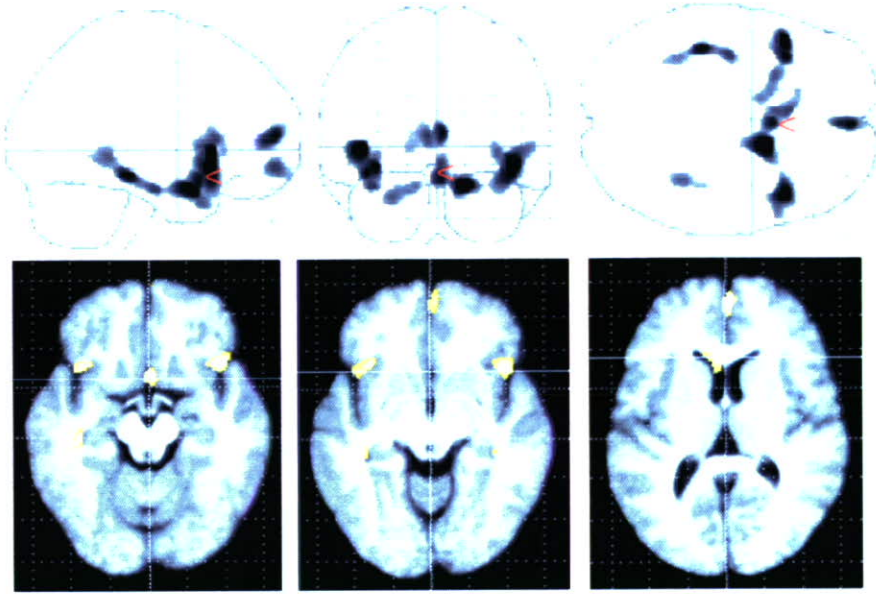

Fig. 4 Increased volumes in schizophrenics as compared to controls. *Top*: The SPM {*t*} is displayed in a standard format as a MIP. Patients with schizophrenia showed a significantly increased volume of the CSF space. *Bottom*: The SPM {*t*} is displayed onto axial T_1-weighted MR images. A significantly increased volume of the CSF space such as the lateral ventricle, sylvian fissures and the interhemisphrenic fissure was noted.

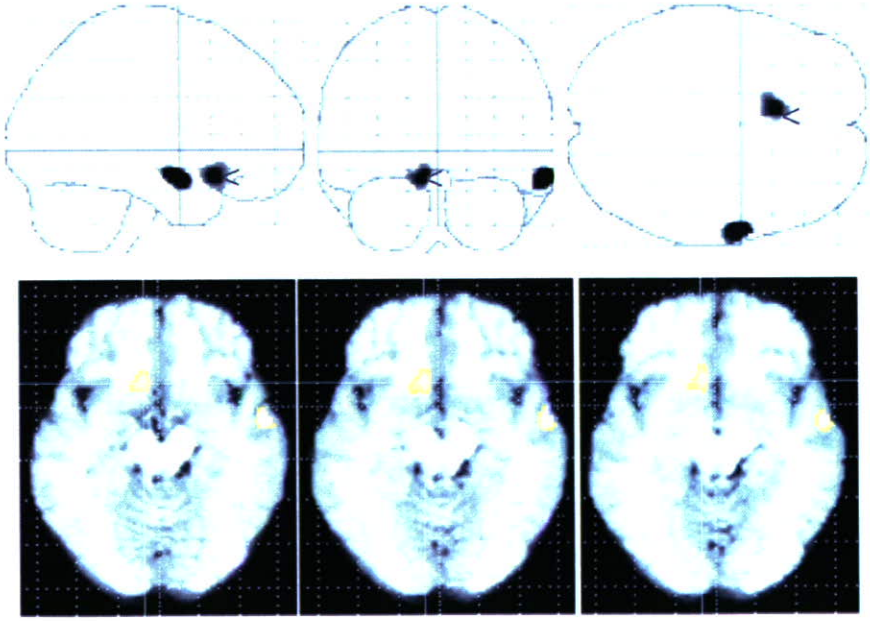

Fig. 5 The result of comparison between individuals homozygous for the Val-COMT allele (n = 57) and Met-COMT carriers (n = 66) (genotype effects). *Top*: Representation in stereotaxic space of regions with significant reduction of volume in individuals homozygous for the Val-COMT allele demonstrated. *Bottom*: The SPM {*t*} is displayed onto axial T_1-weighted MR images. Individuals homozygous for the Val-COMT allele demonstrated a significant reduction of volumes in the left ACC and right MTG as compared to Met-COMT carriers.

In the control group, we found no significant morphological differences between individuals homozygous for the Val-COMT allele and Met-COMT carriers. Even the hypothesis driven analysis with a lenient statistical threshold ($P < 0.05$) could not detect any significant morphological changes in the DLPFC between the two groups. Contrary to the control group, schizophrenics homozygous for the Val-COMT allele showed a significant reduction of volumes in the left amygdala-uncus, bilateral ACC, right MTG and the left thalamus when compared to the patients carrying the Met-COMT

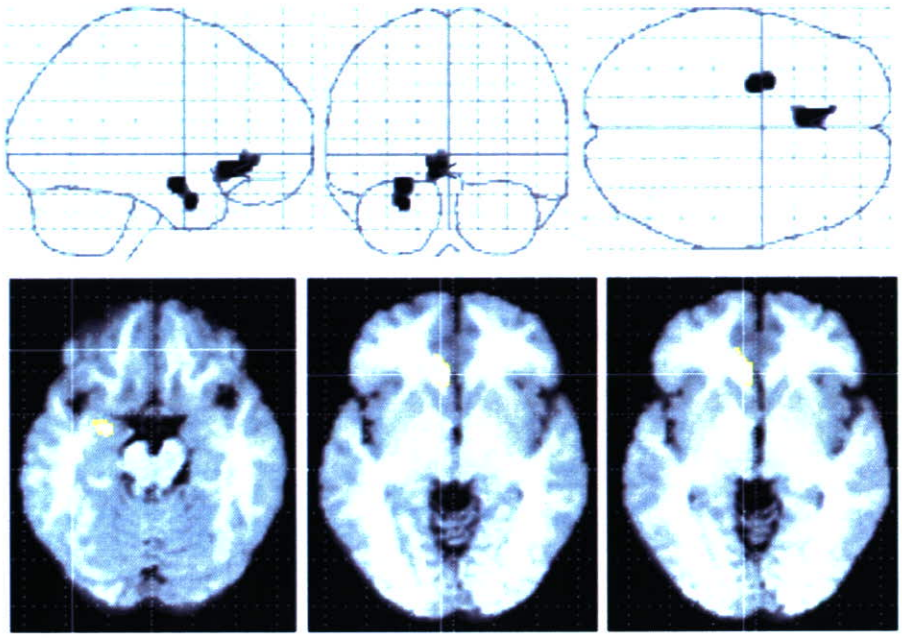

Fig. 6 Results of genotype-diagnosis interaction effects on brain morphology. *Top*: The SPM {*t*} is displayed in a standard format as a MIP. The stronger effects of Val158Met polymorphism on brain morphology in schizophrenia than those in controls were noted in the left ACC, left parahippocampal gyrus and the amygdala-uncus. *Bottom*: The SPM {*t*} is displayed onto axial T_1-weighted MR images.

allele (Table 2, Fig. 7). The hypothesis-driven analysis demonstrated a significantly decreased volume of the bilateral DLPFC in schizophrenics homozygous for the Val-COMT allele when compared to the Met-COMT schizophrenics at a lenient threshold (uncorrected $P = 0.05$) (data not shown). However, no voxels could survive after the correction for multiple comparisons (FDR < 0.05) within the ROI. There are no significantly increased volumes in the schizophrenics homozygous for the Val-COMT allele. All the results were essentially unchanged even if all the left-handed subjects were excluded in all analyses (data not shown).

Discussion

In this study, we found reduction of volumes in the limbic and paralimbic systems, neocortical areas (prefrontal and temporal cortices) and thalamus in patients with schizophrenia when compared to control subjects. The schizophrenia patients demonstrated a significant enlargement of CSF spaces including the lateral and sylvian fissure, which could be interpreted as a result of impaired neurodevelopment and/or global brain atrophy. These findings are concordant with previous studies of MR morphometry of schizophrenia. According to a recent review and meta-analyses of the morphometry of schizophrenia, the consistent abnormalities in schizophrenia are as follows; (i) ventricular enlargement (lateral and third ventricles); (ii) medial temporal lobe involvement; (iii) superior temporal gyrus involvement (iv) parietal lobe involvement; and (v) subcortical brain region involvement including the thalamus (Okubo *et al.*, 2001; Shenton *et al.*, 2001; Davidson and Heinrichs, 2003). The other regions observed in this study, such as the insula, DLPFC and the ACC have also often been demonstrated as abnormal areas in schizophrenia (Shenton *et al.*, 2001; Takahashi *et al.*, 2004; Yamasue *et al.*, 2004). Using the TBM technique, we replicated the morphological abnormalities observed in previous MR studies on schizophrenia, suggesting that TBM was able to detect morphological changes associated with this disease. As well as neuroimaging studies, post-mortem studies have also reported morphological abnormalities in schizophrenia, but not necessarily as common neuropathological features. Regions including the hippocampus, ACC, thalamus and the DLPFC are regularly associated with abnormalities of cell size, cell number and neuronal organization (Bogerts, 1993; Arnold and Trojanowski, 1996; Selemon, 2001; Selemon and Lynn, 2002, 2003). Selemon *et al.* reported that schizophrenics demonstrated abnormalities in overall and laminar neuronal density in the DLPFC (Brodmann area 9) and suggested that the DLPFC should be a particularly vulnerable target in the disease process (Selemon 2001; Selemon and Lynn, 2002, 2003).

Importantly, our results suggest that some of the morphological changes in schizophrenia mentioned above are associated with the Val158Met polymorphism of the COMT gene. In the schizophrenic group, the polymorphism was associated with the volumes in the limbic and paralimbic systems, temporal cortices and the left thalamus, whereas no morphological changes related to the polymorphism were found in

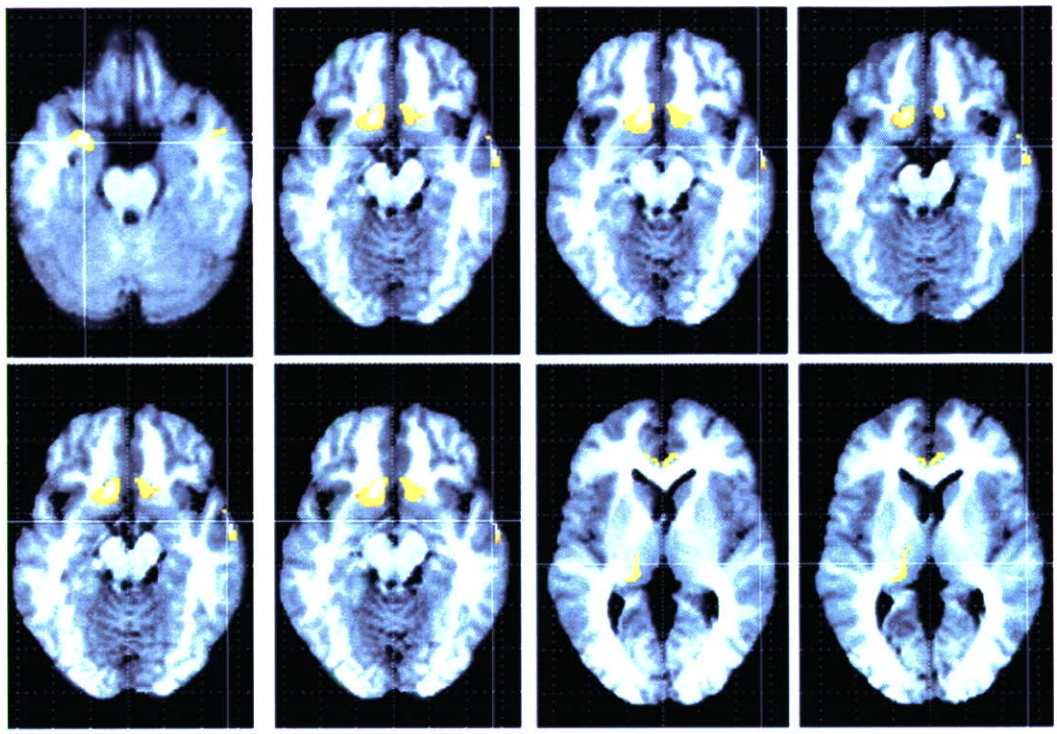

Fig. 7 The effects of the Val158Met polymorphism of the COMT gene on brain morphology in schizophrenics. The SPM {*t*} is displayed onto axial T_1-weighted MR images. The schizophrenics homozygous for the Val-COMT allele (n = 19) showed a significant reduction of volumes in the left parahippocampal gyrus, amygdala-uncus, ACC, left thalamus and the right MTG when compared to patients who carried the Met-COMT allele (n = 28).

normal individuals. As a consequence, significant genotype-diagnosis interaction effects were found in the left ACC and the amygdala-uncus. These results indicate that the Val158-Met polymorphism of the COMT gene is strongly associated with morphological changes in schizophrenia, particularly those in the limbic and paralimbic systems. Longitudinal MRI studies of schizophrenia strongly suggest that progressive changes should occur after onset of the illness (Okubo *et al.*, 2001; Ho *et al.*, 2003). Recent studies have demonstrated that antipsychotic drugs, particularly haloperidol, have considerable effects on brain morphology (Arango *et al.*, 2003; Lieberman, 2005; Dorph *et al.*, 2005). Because of the long duration of illness and medication taken by our subjects, the effects of antipsychotics may be a possible confounding factor for our findings. However, the duration of medication and the dose of antipsychotics taken by the Val/Val-COMT schizophrenics did not differ from those of the Met-COMT schizophrenics. Although the effects of antipsychotics on brain morphology may contribute to the observed morphological changes in patients with schizophrenia in this study, it is unlikely that the effects of antipsychotics contributed to morphological differences between the two schizophrenic groups.

When we were preparing this manuscript, another study demonstrated no genotype and genotype-diagnosis interaction effects of the Val158Met polymorphism on morphology of the frontal lobe in controls and schizophrenia (Ho *et al.*, 2005). Although there are differences between the two studies, such as mean ages of subjects, duration of illness, methods for image analysis and a racial factor (Caucasians versus Japanese), that study also demonstrated no genotype and genotype-diagnosis interaction effects on morphology of the DLPFC. However, we found these effects on DLPFC morphology at a very lenient statistical threshold. Further studies with a larger sample will clarify whether Val158Met polymorphism does affect DLPFC morphology. As well as prefrontal morphology, we found no significant genotype or genotype-diagnosis interaction effects on working memory, however, schizophrenics homozygous for the Val-COMT allele tended to have poorer performances on working memory measures, compared to Met-COMT carriers with schizophrenia. Although there were no significant effects of Val158Met polymorphism on working memory and other neuropsychological measures, a significant effect of the polymorphism was noted in brain morphology. The brain morphology has been considered to be useful as an intermediate phenotype in genetic research in neuropsychiatric disorders (Baare *et al.*, 2001; Durston *et al.*, 2005). Therefore, morphological changes might be more sensitive to the effects of genotype than behavioural measures such as the performance of working memory measures. In a previous study (Ho *et al.*, 2005) a similar phenomenon—no significant effect of Val158Met polymorphism on working memory performance but significant

effects on brain activities during a working memory task—was found. Further studies with a larger sample size are needed to clarify whether morphological changes are a more sensitive marker of genotype effects than behavioural measures.

Unexpectedly, we found effects of the polymorphism on the ACC volume rather than the DLPFC which is crucial for working memory. Since the ACC is associated with a variety of cognitive tasks involving mental efforts, and also plays important roles in working memory (Paus *et al.*, 2001; Kondo *et al.*, 2004), it is feasible that the Val158Met polymorphism may be associated with the ACC morphology. In fact, a previous study demonstrated that the Val-COMT allele was associated with abnormal ACC function as well as abnormal prefrontal cortical function, relative to the Met-COMT allele, as measured by cognitive tests and fMRI activation in normal subjects (Egan *et al.*, 2001).

One would argue that the effects of one polymorphism of the gene could not explain the morphological changes in schizophrenia. As well as the effects of the Val158Met polymorphism, we agree that other polymorphisms of schizophrenia susceptibility genes and genotype–genotype interaction may relate to individual brain morphology. Such interactions might contribute to the different effects of the Val158Met polymorphism on brain morphology observed in this study. Further studies of each effect and interaction of several schizophrenia susceptibility genes on brain morphology, brain functions and performances of neuropsychological tests should be conducted to clarify how polymorphisms of these genes affect intermediate phenotypes of schizophrenia.

In conclusion, we found an association between the Val158Met polymorphism and morphological abnormalities in schizophrenia. Although the underlying mechanisms of our observation remain to be clarified, our data indicate that brain morphology as an intermediate phenotype should be useful for investigating how genotypes affect endophenotypes of schizophrenia.

Acknowledgements

This study was supported by the Promotion of Fundamental Studies in Health Science of Organization for Pharmaceuticals and Medical Devices Agency. This work was also supported in part by Grants-in-Aid from the Japanese Ministry of Health, Labor and Welfare (H17-kokoro-007 and H16-kokoro-002), the Japanese Ministry of Education, Culture, Sports, Science and Technology and Core research for Evolutional Science and Technology of Japan Science and Technology Agency, Japan Foundation for Neuroscience and Mental Health.

References

Arango C, Breier A, McMahon R, Carpenter WT Jr, Buchanan RW. The relationship of clozapine and haloperidol treatment response to prefrontal, hippocampal, and caudate brain volumes. Am J Psychiatry 2003; 160: 1421–7.

Arnold SE, Trojanowski JQ. Recent advances in defining the neuropathology of schizophrenia. Acta Neuropathol (Berl) 1996; 92: 217–31.

Ashburner J, Friston KJ. High-dimensional image warping. In: Frackowiak R, editor. Human brain function. 2nd edn. Academic Press; 2004. p. 673–94.

Baare WF, Hulshoff Pol HE, Boomsma DI, Posthuma D, de Geus EJ, Schnack HG, et al. Quantitative genetic modeling of variation in human brain morphology. Cereb Cortex 2001; 11: 816–24.

Bogerts B. Recent advances in the neuropathology of schizophrenia. Schizophr Bull 1993; 19: 431–45.

Cannon TD, Mednick SA, Parnas J, Schulsinger F, Praestholm J, Vestergaard A. Developmental brain abnormalities in the offspring of schizophrenic mothers. I. Contributions of genetic and perinatal factors. Arch Gen Psychiatry 1993; 50: 551–64.

Chen J, Lipska BK, Halim N, Ma QD, Matsumoto M, Melhem S, et al. Functional analysis of genetic variation in catechol-O-methyltransferase (COMT): effects on mRNA, protein, and enzyme activity in postmortem human brain. Am J Hum Genet 2004; 75: 807–21.

Daniels JK, Williams NM, Williams J, Jones LA, Cardno AG, Murphy KC, et al. No evidence for allelic association between schizophrenia and a polymorphism determining high or low catechol O-methyltransferase activity. Am J Psychiatry 1996; 153: 268–70.

Davidson LL, Heinrichs RW. Quantification of frontal and temporal lobe brain-imaging findings in schizophrenia: a meta-analysis. Psychiatry Res 2003; 122: 69–87.

Dorph Petersen KA, Pierri JN, Perel JM, Sun Z, Sampson AR, Lewis DA. The influence of chronic exposure to antipsychotic medications on brain size before and after tissue fixation: a comparison of haloperidol and olanzapine in macaque monkeys. Neuropsychopharmacology 2005; 30: 1649–61.

Durston S, Fossella JA, Casey BJ, Hulshoff Pol HE, Galvan A, Schnack HG, et al. Differential effects of DRD4 and DAT1 genotype on fronto-striatal gray matter volumes in a sample of subjects with attention deficit hyperactivity disorder, their unaffected siblings, and controls. Mol Psychiatry 2005; 10: 678–85.

Egan MF, Goldberg TE, Kolachana BS, Callicott JH, Mazzanti CM, Straub RE, et al. Effect of COMT Val108/158 Met genotype on frontal lobe function and risk for schizophrenia. Proc Natl Acad Sci USA 2001; 98: 6917–22.

Fan JB, Zhang CS, Gu NF, Li XW, Sun WW, Wang HY, et al. Catechol-O-methyltransferase gene Val/Met functional polymorphism and risk of schizophrenia: a large-scale association study plus meta-analysis. Biol Psychiatry 2005; 57: 139–44.

Galderisi S, Maj M, Kirkpatrick B, Piccardi P, Mucci A, Invernizzi G, et al. COMT Val(158)Met and BDNF C(270) T polymorphisms in schizophrenia: a case-control study. Schizophr Res 2005; 73: 27–30.

Gaser C, Nenadic I, Buchsbaum BR, Hazlett EA, Buchsbaum MS. Deformation-based morphometry and its relation to conventional volumetry of brain lateral ventricles in MRI. Neuroimage 2001; 13: 1140–5.

Gogtay N, Sporn A, Clasen LS, Greenstein D, Giedd JN, Lenane M, et al. Structural brain MRI abnormalities in healthy siblings of patients with childhood-onset schizophrenia. Am J Psychiatry 2003; 160: 569–571.

Goldberg TE, Egan MF, Gscheidle T, Coppola R, Weickert T, Kolachana BS, et al. Executive subprocesses in working memory: relationship to catechol-O-methyltransferase Val158Met genotype and schizophrenia. Arch Gen Psychiatry 2003; 60: 889–96.

Gurtin, ME. An introduction to continuum mechanics. Boston: Academic Press; 1987.

Harrison PJ, Weinberger DR. Schizophrenia genes, gene expression, and neuropathology: on the matter of their convergence. Mol Psychiatry 2005; 10: 40–68.

Hashimoto R, Yoshida M, Ozaki N, Yamanouchi Y, Iwata N, Suzuki T, et al. Association analysis of the -308G>A promoter polymorphism of the tumor necrosis factor alpha (TNF-alpha) gene in Japanese patients with schizophrenia. J Neural Transm 2004; 111: 217–21.

Hashimoto R, Yoshida M, Kunugi H, Ozaki N, Yamanouchi Y, Iwata N, et al. A missense polymorphism (H204R) of a Rho GTPase-activating protein, the chimerin 2 gene, is associated with schizophrenia in men. Schizophr Res 2005; 73: 383–5.

Ho BC, Andreasen NC, Nopoulos P, Arndt S, Magnotta V, Flaum M. Progressive structural brain abnormalities and their relationship to clinical outcome: a longitudinal magnetic resonance imaging study early in schizophrenia. Arch Gen Psychiatry 2003; 60: 585–94.

Ho BC, Wassink TH, O'leary DS, Sheffield VC, Andreasen NC. Catechol-O-methyl transferase Val(158)Met gene polymorphism in schizophrenia: working memory, frontal lobe MRI morphology and frontal cerebral blood flow. Mol Psychiatry 2005; 10: 287–98.

Kendler KS. Overview: a current perspective on twin studies of schizophrenia. Am J Psychiatry 1983; 140: 1413–25.

Kondo H, Osaka N, Osaka M. Cooperation of the anterior cingulate cortex and dorsolateral prefrontal cortex for attention shifting. Neuroimage 2004; 23: 670–9.

Kunugi H, Vallada HP, Sham PC, Hoda F, Arranz MJ, Li T, et al. Catechol-O-methyltransferase polymorphisms and schizophrenia: a transmission disequilibrium study in multiply affected families. Psychiatr Genet 1997; 7: 97–101.

Lieberman JA, Tollefson GD, Charles C, Zipursky R, Sharma T, Kahn RS, et al. Antipsychotic drug effects on brain morphology in first-episode psychosis. Arch Gen Psychiatry 2005; 62: 361–70.

Maldjian JA, Laurienti PJ, Kraft RA, Burdette JH. An automated method for neuroanatomic and cytoarchitectonic atlas-based interrogation of fMRI data sets. Neuroimage 2003; 19: 1233–9.

McGue M, Gottesman II, Rao DC. The transmission of schizophrenia under a multifactorial threshold model. Am J Hum Genet 1983; 35: 1161–78.

Nelson KB, Lynch JK. Stroke in newborn infants. Lancet Neurol 2004; 3: 150–8.

Norton N, Kirov G, Zammit S, Jones G, Jones S, Owen R, et al. Schizophrenia and functional polymorphisms in the MAOA and COMT genes: no evidence for association or epistasis. Am J Med Genet 2002; 114: 491–6.

Ohmori O, Shinkai T, Kojima H, Terao T, Suzuki T, Mita T, et al. Association study of a functional catechol-O-methyltransferase gene polymorphism in Japanese schizophrenics. Neurosci Lett 1998; 243: 109–12.

Okubo Y, Saijo T, Oda K. A review of MRI studies of progressive brain changes in schizophrenia. J Med Dent Sci 2001; 48: 61–7.

Palmatier MA, Kang AM, Kidd KK. Global variation in the frequencies of functionally different catechol-O-methyltransferase alleles. Biol Psychiatry 1999; 46: 557–67.

Paus T. Primate anterior cingulate cortex: where motor control, drive and cognition interface. Nat Rev Neurosci 2001; 2: 417–24.

Pezawas L, Verchinski BA, Mattay VS, Callicott JH, Kolachana BS, Straub RE, et al. The brain-derived neurotrophic factor val66met polymorphism and variation in human cortical morphology. J Neurosci 2004; 24: 10099–102.

Selemon LD. Regionally diverse cortical pathology in schizophrenia: clues to the etiology of the disease. Schizophr Bull 2001; 27: 349–77.

Shenton ME, Dickey CC, Frumin M, McCarley RW. A review of MRI findings in schizophrenia. Schizophr Res 2001; 49: 1–52.

Steel RM, Whalley HC, Miller P, Best JJ, Johnstone EC, Lawrie SM. Structural MRI of the brain in presumed carriers of genes for schizophrenia, their affected and unaffected siblings. J Neurol Neurosurg Psychiatry 2002; 72: 455–8.

Stefanis NC, Van Os J, Avramopoulos D, Smyrnis N, Evdokimidis I, Hantoumi I, et al. Variation in catechol-O-methyltransferase val158 met genotype associated with schizotypy but not cognition: a population study in 543 young men. Biol Psychiatry 2004; 56: 510–5.

Sullivan PF, Kendler KS, Neale MC. Schizophrenia as a complex trait: evidence from a meta-analysis of twin studies. Arch Gen Psychiatry 2003; 60: 1187–92.

Takahashi T, Suzuki M, Hagino H, Zhou SY, Kawasaki Y, Nohara S, et al. Bilateral volume reduction of the insular cortex in patients with schizophrenia: a volumetric MRI study. Psychiatry Res 2004; 132: 187–96.

Talairach J, Tournoux P. A coplanar stereotaxic atlas of a human brain. Three-dimensional proportional system: an approach to cerebral imaging. Stuttgart: Thieme; 1988.

Tunbridge EM, Bannerman DM, Sharp T, Harrison PJ. Catechol-O-methyltransferase inhibition improves set-shifting performance and elevates stimulated dopamine release in the rat prefrontal cortex. J Neurosci 2004; 24: 5331–5.

Weinberger DR, Egan MF, Bertolino A, Callicott JH, Mattay VS, Lipska BK, et al. Prefrontal neurons and the genetics of schizophrenia. Biol Psychiatry 2001; 50: 825–44.

Wright IC, McGuire PK, Poline JB, Travere JM, Murray RM, Frith CD, et al. A voxel-based method for the statistical analysis of gray and white matter density applied to schizophrenia. Neuroimage 1995; 2: 244–52.

Yamasue H, Iwanami A, Hirayasu Y, Yamada H, Abe O, Kuroki N, et al. Localized volume reduction in prefrontal, temporolimbic, and paralimbic regions in schizophrenia: an MRI parcellation study. Psychiatry Res 2004; 131: 195–207.

Journal of Cerebral Blood Flow & Metabolism (2006), 1–7
 0271-678X/06 $30.00
www.jcbfm.com

Estimation of oxygen metabolism in a rat model of permanent ischemia using positron emission tomography with injectable ^{15}O-O_2

Takashi Temma[1], Yasuhiro Magata[2], Yuji Kuge[1], Sayaka Shimonaka[1], Kohei Sano[1], Yumiko Katada[1], Hidekazu Kawashima[3], Takahiro Mukai[3], Hiroshi Watabe[4], Hidehiro Iida[4] and Hideo Saji[1]

[1]*Department of Patho-Functional Bioanalysis, Graduate School of Pharmaceutical Sciences, Kyoto University, Kyoto, Japan;* [2]*Laboratory of Genome Bio-Photonics, Photon Medical Research Center, Hamamatsu University School of Medicine, Hamamatsu, Japan;* [3]*Department of Nuclear Medicine and Diagnostic Imaging, Graduate School of Medicine, Kyoto University, Kyoto, Japan;* [4]*Department of Investigative Radiology, National Cardiovascular Center Research Institute, Suita, Japan*

The threshold of cerebral blood flow (CBF) into infarction in rats has been indicated to be similar to that in patients. However, CBF does not reflect metabolic function, and so estimations of oxygen metabolism have been required. Here, we estimated changes in oxygen metabolism after occluding the right middle cerebral artery (MCA) in rats using an injectable ^{15}O-O_2 we developed. A decrease in CBF (left: 0.67±0.22 mL/min/g, right: 0.44±0.17 mL/min/g, $P<0.05$) and compensatory increase in the oxygen extraction fraction (OEF) (left: 0.42±0.13, right: 0.50±0.19, $P<0.05$) were observed at 1-h after occlusion. In contrast, a marked decrease in CBF and the cerebral metabolic rate for oxygen and a collapse of the compensatory OEF mechanism were found at 24 h after occlusion. Injectable ^{15}O-O_2 could be used to reliably estimate oxygen metabolism in an infarction rat model with positron emission tomography.
Journal of Cerebral Blood Flow & Metabolism advance online publication, 22 March 2006; doi:10.1038/sj.jcbfm.9600302

Keywords: OEF; oxygen metabolism; permanent ischemia; positron emission tomography; rat

Introduction

Stroke is closely related to alterations in cerebral blood flow (CBF), the cerebral metabolic rate for oxygen ($CMRO_2$), the oxygen extraction fraction (OEF), cerebral blood volume, and so on while some neurodegenerative disorders such as Alzheimer's disease and Parkinson's disease are also reported to induce a change in CBF (Derejko *et al*, 2001; Mori, 2002) because of tissue degradation. Therefore, estimation of these circulatory and metabolic parameters is important for both pathophysiological studies and the development or evaluation of new methods for treating stroke.

Studies on changes in parameters of cerebral circulation after the onset of stroke have been performed in several animal models (Belayev *et al*, 1997; Ginsberg, 2003; Heiss *et al*, 1997, 1994; Pappata *et al*, 1993; Takamatsu *et al*, 2000; Tenjin *et al*, 1992; Young *et al*, 1996; Zhao *et al*, 1997) and patients (Baron, 2001; Heiss *et al*, 2001). In the studies using larger animals, CBF, OEF and $CMRO_2$ were estimated after the onset of ischemia by positron emission tomography (PET) with ^{15}O-H_2O and ^{15}O-O_2 gas and used as predictors for the progression of brain infarction. These reports indicated that areas showing a decrease in CBF and compensatory increase in OEF in the early phase of stroke were vital several hours after the onset. Also, in studies with rats as an animal model of ischemia, CBF was certainly indicated to be a good predictor for infarction in comparison with the results for

Correspondence: Dr Y Magata, Laboratory of Genome Bio-Photonics, Photon Medical Research Center, Hamamatsu University School of Medicine, 1-20-1 Handayama, Hamamatsu 431-3192, Japan.
E-mail: magata@hama-med.ac.jp
This study was partly supported by Mitsubishi Pharma Research Foundation. This work was also supported by Grants-in-Aid for Scientific Research and by the 21st Century Center of Excellence Program at Kyoto University 'Knowledge Information Infrastructure for Genome Science' and at Hamamatsu University School of Medicine 'Medical Photonics' from the Ministry of Education, Culture, Sports, Science and Technology, Japan.
Received 4 October 2005; revised 7 February 2006; accepted 10 February 2006

patients (Belayev *et al*, 1997; Ginsberg, 2003; Zhao *et al*, 1997). However, CBF does not reflect cell energy metabolism and so measurements of oxygen metabolism are required to accurately estimate tissue viability. Additionally, since that there are functional differences between rodents and humans (Walovitch *et al*, 1994), careful evaluation is needed when using rats to investigate the pathophysiology and progression of human stroke. On these bases, we adopted MCA occluded rats, widely used ischemia model (Kuge *et al*, 1995; Longa *et al*, 1989; Minematsu *et al*, 1992), and evaluated the changes in CBF, OEF and $CMRO_2$ after the onset of stroke with PET.

On the other hand we recently developed a method of measuring regional OEF in the rat brain noninvasively using PET (Magata *et al*, 2003). Here, we designed experiments to estimate CBF, OEF and $CMRO_2$ by PET in the early and late phases of a permanent ischemia in rats.

Materials and methods

Animals

Male Sprague–Dawley rats (250 to 310 g) supplied by Japan SLC Co. (Hamamatsu, Japan) were housed for 1 week under a 12-h light/12-h dark cycle and given free access to food and water. The animal experiments in this study were conducted in accordance with institutional guidelines and approved by the Kyoto University Animal Care Committee.

Preparation of ^{15}O-Labeled Compounds

The production of ^{15}O-H_2O and injection of ^{15}O-oxygen (injectable ^{15}O-O_2) were conducted as reported previously (Magata *et al*, 2003). Briefly, ^{15}O-H_2O was synthesized by the reduction of ^{15}O-O_2 with H_2 gas (catalyzed by Pd black at 140°C) and trapped in a saline solution. As for injectable ^{15}O-O_2, part of an infusion line kit (Terumo Corporation, Tokyo, Japan) used as a blood reservoir and an artificial lung 18 cm in length (Senko Medical Instrument Mfg Co. Ltd, Tokyo, Japan) designed for small animals such as rats were connected to a peristaltic pump (EYELA roller pump RP-1000, Tokyo Rikakikai Co. Ltd, Tokyo, Japan) to make a closed system. Then, 18 to 20 mL of blood was collected from several rats and filtered with saline-wetted gauze. The blood was circulated (100 mL/min) in the system and ^{15}O-O_2 gas (4100 to 5100 MBq/min/500 ml) was introduced into the artificial lung to prepare injectable ^{15}O-O_2 (51 to 90 MBq/ml).

Animal Preparation

Rats were divided into two groups. One was for the early phase PET experiment ($n=7$, 1 h after the onset of occlusion) and the other was for the late phase experiment ($n=6$, 24 h after the onset of occlusion). The rats were starved for 6 h before the operation and anesthetized with chloral hydrate (i.p. 400 mg/kg). For the early phase group, anesthesia was sustained throughout the experiment. The left femoral artery in each rat was catheterized using a PE 20 catheter (i.d. 0.5 mm, o.d. 0.8 mm) for blood sampling during PET study. Then, the right middle cerebral artery (MCA) was occluded intraluminally using a nylon 4-0 monofilament (Kuge *et al*, 1995; Longa *et al*, 1989; Minematsu *et al*, 1992). For the late phase group, each rat was aroused from anesthesia after the right MCA occlusion and then anesthetized for the catheterization of the left femoral artery and PET experiments. After the completion of the operation, rats were administered i.v. with 100 IU of heparin. The animal was placed supine in a stereotaxic apparatus, and its head was restrained by mouth and ear bars. After the acquisition of a blank scan for 180 mins, the apparatus was placed in a PET camera (SHR-7700L, Hamamatsu Photonics, Hamamatsu, Japan) (Watanabe *et al*, 1997). The position was standardized with the aid of a laser beam, and the desired cranial position in the camera was oriented. Rectal temperature was maintained at around 37 °C with the aid of heating pads and blood gases were measured using a blood gas analyzer (Rapidlab 348, Chiron Diagnostics Ltd, Essex, England) several times during the experiment. After the PET experiments, 2,3,5-triphenyltetrazolium chloride (TTC) staining was performed in some cases for evaluating the progression of stroke.

Positron Emission Tomography Experiments

A transmission scan was performed for 30 mins for attenuation correction following the blank scan. Then, a dynamic PET scan was performed using ^{15}O-H_2O (i.v., 148 to 185 MBq) to measure CBF values 1 h or 24 h after the initiation of MCA occlusion. A second PET scan was performed with the administration of injectable ^{15}O-O_2 (i.v., 74 to 148 MBq) over a 60-secs period to measure OEF values after the radioactivity of ^{15}O-H_2O had decayed in the body. In both cases, the total scan acquisition period was 120 secs and the scan consisted of 12 × 10-second frames. Arterial blood sampling was performed continuously throughout the PET scans and blood centrifugation was also performed for measuring the plasma concentration of ^{15}O radioactivity. The radioactivity of each sample was measured with an NaI well scintillation counter (Packard AutoGamma 500, Packard Instruments, Meriden, CT, USA) calibrated using a ^{22}Na standard radioactive source.

Data Analysis

Positron emission tomography images were obtained as described previously (Magata *et al*, 2003). The rat brain was visualized in four consecutive coronal slices. Then, two regions of interest (ROIs) in each slice, right and left hemispheres, were visually chosen according to the magnetic resonance images obtained previously in the another study using 1.5T MRI. Activity in ROIs was calibrated using a cross calibration factor calculated in